

Some Theory for Texture Segmentation

Lin Zheng

Abstract

In the context of texture segmentation in images, and provide some theoretical guarantees for the prototypical approach which consists in extracting local features in the neighborhood of a pixel and then applying a clustering algorithm for grouping the pixel according to these features. On the one hand, for stationary textures, which we model with Gaussian Markov random fields, we construct the feature for each pixel by calculating the sample covariance matrix of its neighborhood patch and cluster the pixels by an application of k-means to group the covariance matrices. We show that this generic method is consistent. On the other hand, for non-stationary fields, we include the location of the pixel as an additional feature and apply single-linkage clustering. We again show that this generic and emblematic method is consistent. We complement our theory with some numerical experiments performed on both generated and natural textures.

1 Introduction

Texture segmentation fits within the larger area of image segmentation, with a particular focus on images that contain textures. The goal, then, is to partition the image, i.e., group the pixels, into differently textured regions. Texture segmentation, and image segmentation more generally, is an important task in computer vision and pattern recognition, being widely applied to areas such as scene understanding, remote sensing and autonomous driving (Liu et al., 2019; Pal and Pal, 1993; Reed and Dubuf, 1993; Zhang, 2006).

At least in recent decades, texture segmentation methods are almost invariably based on extracting local features around each pixel, such as SIFT (Lowe, 1999), which are then fed into a clustering algorithm, such as k-means. An emblematic approach in this context is that of Shi and Malik (2000), who used the pixel value as feature, arguably the simplest possible choice, and applied a form of spectral clustering to group the pixels. The process is similar to what is done in the adjacent area of texture classification, the main difference being that a classification method is used instead of a clustering algorithm (Randen and Husoy, 1999a; Varma, 2004).

Although this basic approach has remained essentially unchanged, the process of extracting features has undergone some important changes over the years, ranging from the use of sophisticated systems from applied harmonic analysis such as Gabor filters or wavelets (Dunn and Higgins, 1995; Grigorescu et al., 2002; Jain and Farrokhnia, 1991; Randen and Husoy, 1999b; Unser, 1995; Weldon and Higgins, 1996) to multi-resolution or multiscale aggregation approaches (Galun et al., 2003; Mao and Jain, 1992), among others (Hofmann et al., 1998; Malik et al., 2001), to the use deep learning, particularly in the form convolutional neural networks (CNN), whose success is attributed to the capability of CNN to learn a hierarchical representation of raw input data (Badrinarayanan et al.,

The author is with the Department of Mathematics, University of California, San Diego, USA. Contact information is available [here](#).

2017; Long et al., 2015; Milletari et al., 2016; Ronneberger et al., 2015). See (Humeau-Heurtier, 2019) for a recent survey.

While the vast majority of the work in texture segmentation, as in image processing at large, is applied, we contribute some theory by establishing the consistency of the basic approach described above. We do so in a stylized setting which is nonetheless a reasonable mathematical model for the problem of texture segmentation. Markov random fields (MRF) are common models for textures (Cross and Jain, 1983; Geman and Graffigne, 1986), and arguably the most popular in theoretical texture analysis (Arias-Castro et al., 2018; Rue and Held, 2005; Verzelen, 2010a,b; Verzelen and Villers, 2009). This is the model that we use. Although supplanted by the more recent feature extraction methods mentioned above, which in recent years are invariably nonparametric, Gaussian MRF in particular remain the most commonly-used parametric model for textures, also used in the development of methodology not too long ago (Chellappa and Chatterjee, 1985; Manjunath and Chellappa, 1991; Paciorek and Schervish, 2006; Zhu et al., 1998). When textures are modeled by stationary Gaussian MRF, what characterizes them is the covariance structure, so that in congruence with adopting Gaussian MRF as models for textures, when assumed stationary the feature we extract is the (local) covariance. When textures are not assumed stationary, we also incorporate location as an additional feature, as the covariance structure may change within a textured region.

The basic approach calls for applying a clustering algorithm to the extracted features. Features are typically represented by (possibly high-dimensional) feature vectors, as is the case with the features that we work with, and thus a large number of clustering methods are applicable, some of them coming with theoretical guaranties such as k-means (Arthur and Vassilvitskii, 2007), Gaussian mixture models (Dasgupta, 1999; Hsu and Kakade, 2013; Vempala and Wang, 2004), hierarchical clustering (Dasgupta, 2010; Dasgupta and Long, 2005), including single-linkage clustering (Arias-Castro, 2011), and spectral clustering (Ng et al., 2002). In this paper, we use k-means in the context of stationary textures and single-linkage clustering in the context of non-stationary textures.

The paper is organized as follows. In Section 2, we consider stationary textures, which is done by the extraction of local second moment information on patches and the application of k-means. In Section 3, we consider non-stationary textures, where we also include location as a feature and we apply instead single-linkage clustering. In Section 4, we present the result of some numerical experiments, mostly there to illustrate the theory developed in the main part of the paper. Both synthetic and natural textures are considered.

2 Stationary Textures

In this section we consider textures to be stationary. The model we adopt and the method we implement are introduced in Section 2.1 and Section 2.2. We then establish in Section 2.3 the consistency of a simple incarnation of the basic approach.

2.1 Model

We have a pixel image X of size $n \times n$, that we assume is partitioned into two sub-regions \mathcal{G}_0 and \mathcal{G}_1 by curve $\bar{\mathcal{G}}$. \mathcal{G}_0 is a stationary Gaussian Markov random field with mean 0 and autocovariance matrix A_0 . \mathcal{G}_1 is a stationary Gaussian Markov random field with mean 0 and autocovariance matrix A_1 . In image X , we pick up n^2 pixels with equal intervals, and get observations

$$\{X_t\}, \quad t \in \mathcal{T} := \{1, 2, \dots, n\}^2. \quad (1)$$

To estimate curve $\bar{\mathcal{G}}$, we need to cluster the n^2 pixels into two groups.

2.2 Methods

We define scanning patches as follows. To simplify the presentation assume n is the square of an integer (namely $n = m^2$ for some integer m). For $\forall t = (t_1, t_2) \in \mathcal{T}$, pick up patch S_t with size $(2m + 1) \times (2m + 1)$,

$$S_t = \begin{pmatrix} X_{t+(-m,-m)} & X_{t+(-m,-m+1)} & \cdots & X_{t+(-m,m)} \\ X_{t+(-m+1,-m)} & X_{t+(-m+1,-m+1)} & \cdots & X_{t+(-m+1,m)} \\ \vdots & \vdots & \cdots & \vdots \\ X_{t+(m,-m)} & X_{t+(m,-m+1)} & \cdots & X_{t+(m,m)} \end{pmatrix}, \quad (2)$$

Next, autocovariance is defined based on scanning patches. For $\forall t = (t_1, t_2) \in \mathcal{T}$ and $\forall i = (i_1, i_2) \in \mathcal{M} := \{-m, -m + 1, \dots, m - 1, m\}^2$, define true autocovariance and sample autocovariance as follows

$$C_t(i) = \text{Mean of } \{\mathbb{E}(X_t \cdot X_{t+i}) \mid \text{both } X_t \text{ and } X_{t+i} \text{ are in } S_t\}, \quad (3)$$

$$\hat{C}_t(i) = \text{Mean of } \{X_t \cdot X_{t+i} \mid \text{both } X_t \text{ and } X_{t+i} \text{ are in } S_t\}. \quad (4)$$

Denote the vectorizations of $\{C_t(i)\}_{i \in \mathcal{M}}$ and $\{\hat{C}_t(i)\}_{i \in \mathcal{M}}$ to be C_t and \hat{C}_t respectively. Here C_t is the true feature of pixel X_t and \hat{C}_t is the observed feature of pixel X_t .

Also based on scanning patches, we define following three sets

$$\mathcal{H}_0 = \{t \in \mathcal{T} \mid S_t \subset \mathcal{G}_0\}, \quad (5)$$

$$\mathcal{H}_1 = \{t \in \mathcal{T} \mid S_t \subset \mathcal{G}_1\}, \quad (6)$$

$$\mathcal{H} = \{t \in \mathcal{T} \mid S_t \cap \mathcal{G}_0 \neq \emptyset \text{ and } S_t \cap \mathcal{G}_1 \neq \emptyset\}. \quad (7)$$

Here \mathcal{G}_0 and \mathcal{G}_1 are both stationary fields, so all elements in set $\{C_t\}_{\forall t \in \mathcal{H}_0}$ are the same and we denote it as C^0 . Similarly, all elements in set $\{C_t\}_{\forall t \in \mathcal{H}_1}$ are the same and we denote it as C^1 .

Define template autocovariance $E = \begin{pmatrix} C^0 \\ C^1 \end{pmatrix}$.

Then we introduce membership matrix. Define $n^2 \times 2$ true membership matrix W such that for $\forall t = (t_1, t_2) \in \mathcal{T}$,

$$W_t = \text{the } n(t_1 - 1) + t_2 \text{ th row of matrix } W = \begin{cases} (1, 0), & \text{if } t = (t_1, t_2) \in \mathcal{G}_0, \\ (0, 1), & \text{if } t = (t_1, t_2) \in \mathcal{G}_1. \end{cases} \quad (8)$$

Also define the set of membership matrices $\mathcal{W}_{n,2}$ as follows

$$\mathcal{W}_{n,2} = \{n^2 \times 2 \text{ matrices with rows } (0, 1) \text{ or } (1, 0)\}. \quad (9)$$

Based on above calculations and definitions, we define k-means clustering estimation as

$$(\hat{W}, \hat{E}) = \arg \min_{W \in \mathcal{W}_{n,2}, E \in \mathbb{R}_{2 \times (2m+1)^2}} \sum_{t \in \mathcal{T}} \|(WE)_t - \hat{C}_t\|_\infty^2, \quad (10)$$

where $(WE)_t$ is the $n(t_1 - 1) + t_2$ th row of matrix WE .

In practice k-means can not be solved exactly, however, there exists polynomial time algorithm which obtains approximation (\hat{W}, \hat{E}) satisfying following equation (11), such as $(1 + \epsilon)$ -approximate method in (Kumar et al., 2004).

$$\sum_{t \in \mathcal{T}} \|(\hat{W}\hat{E})_t - \hat{C}_t\|_\infty^2 \leq (1 + \epsilon) \cdot \min_{W \in \mathcal{W}_{n,2}, E \in \mathbb{R}_{2 \times (2m+1)^2}} \sum_{t \in \mathcal{T}} \|(WE)_t - \hat{C}_t\|_\infty^2, \quad (11)$$

where $\hat{W} \in \mathcal{W}_{n,2}$ and $\hat{E} \in \mathbb{R}_{2 \times (2m+1)^2}$. Thus we cluster the n^2 pixels into two groups by membership matrix estimation \hat{W} . As a summary, we provide the procedure of k-means algorithm in Algorithm 1.

Algorithm 1 Texture Segmentation with K-means Algorithm

Input: Observations $\{X_t\}_{t \in \mathcal{T}}$, approximation error ϵ .

Output: Membership matrix estimation \hat{W} .

- 1: For $\forall t = (t_1, t_2) \in \mathcal{T}$, pick up patch S_t .
 - 2: Calculate sample autocovariance $\{\hat{C}_t(i)\}_{i \in \mathcal{M}}$ and obtain observed features $\{\hat{C}_t\}_{t \in \mathcal{T}}$.
 - 3: Define template autocovariance E and the set of membership matrices $\mathcal{W}_{n,2}$.
 - 4: Obtain k-means approximation solution (\hat{W}, \hat{E}) which satisfies (11).
 - 5: **return** \hat{W} .
-

Define the set of 2×2 permutation matrices

$$\Phi_2 = \left\{ \begin{pmatrix} 1 & 0 \\ 0 & 1 \end{pmatrix}, \begin{pmatrix} 0 & 1 \\ 1 & 0 \end{pmatrix} \right\}, \quad (12)$$

then calculate

$$\hat{Q} = \arg \min_{Q \in \Phi_2} \sum_{t \in \mathcal{T}} \|(\hat{W}Q)_t - W_t\|_\infty^2. \quad (13)$$

Next, define the set of mistakenly clustered elements to be \mathcal{R} as follows

$$\mathcal{R} = \{t \in \mathcal{T} : (\hat{W}\hat{Q})_t \neq W_t\}, \quad (14)$$

then clustering error rate is

$$|\mathcal{R}|/n^2 = \frac{1}{n^2} \sum_{t \in \mathcal{T}} \|(\hat{W}\hat{Q})_t - W_t\|_\infty^2. \quad (15)$$

2.3 Theory

Firstly we introduce following assumptions.

Assumption 1. Both \mathcal{G}_0 and \mathcal{G}_1 are wide-sense stationary Gaussian Markov random fields.

Assumption 2. Let $\Delta = \|C^0 - C^1\|_\infty$. For $\forall \beta > 1$,

$$\frac{(\log n)^\beta}{\Delta^2 n} \rightarrow 0 \quad \text{as } n \rightarrow \infty. \quad (16)$$

Assumption 3. Define $C_{t0} = C^0$ for $\forall t \in \mathcal{G}_0$ and $C_{t0} = C^1$ for $\forall t \in \mathcal{G}_1$. With the same β in Assumption 2,

$$\sum_{t \in \mathcal{H}} \|C_t - C_{t0}\|_\infty^2 \leq \frac{n(\log n)^\beta}{24}. \quad (17)$$

Next, before introducing the theory, we indicate the error bound of $\|\hat{C}_t - C_t\|_\infty$.

Lemma 2.1. *Under Assumption 1, for $\forall t \in \mathcal{T}$ and $\forall a > 0$, there exists a constant J such that*

$$\mathbb{P}(\|\hat{C}_t - C_t\|_\infty > a) \leq 2(2\sqrt{n} + 1)^2 \exp(-J \cdot a^2 n). \quad (18)$$

Proof. First let S_t^v be the vectorization of S_t , then S_t^v is a vector of length $(2m+1)^2$

$$S_t^v = \begin{pmatrix} X_{t+(-m,-m)} \\ \vdots \\ X_{t+(-m,m)} \\ X_{t+(-m+1,-m)} \\ \vdots \\ X_{t+(-m+1,m)} \\ \vdots \\ \vdots \\ \vdots \\ X_{t+(m,-m)} \\ \vdots \\ X_{t+(m,m)} \end{pmatrix}. \quad (19)$$

Then for $\forall i = (i_1, i_2) \in \mathcal{M}$, there exists a matrix A_i such that

$$\hat{C}_t(i) = \frac{1}{(2m+1-|i_1|)(2m+1-|i_2|)} (S_t^v)^T A_i S_t^v, \quad (20)$$

where A_i is a $(2m+1)^2 \times (2m+1)^2$ matrix with elements 0 and 1, and the number of 1 is less than $(2m+1-|i_1|)(2m+1-|i_2|)$.

Since the field is stationary, suppose $S_t^v \sim N(0, \Sigma)$, where Σ is non-negative. Let $\Sigma = U\Lambda U^T$ be the spectral decomposition of Σ . Define

$$Y_t = U^T S_t^v, \quad (21)$$

then

$$Y_t \sim N(0, U^T \Sigma U) = N(0, \Lambda). \quad (22)$$

So

$$\hat{C}_t(i) = \frac{1}{(2m+1-|i_1|)(2m+1-|i_2|)} (S_t^v)^T A_i S_t^v \quad (23)$$

$$= \frac{1}{(2m+1-|i_1|)(2m+1-|i_2|)} (UY_t)^T A_i (UY_t) \quad (24)$$

$$= \frac{1}{(2m+1-|i_1|)(2m+1-|i_2|)} Y_t^T (U^T A_i U) Y_t. \quad (25)$$

By Hanson-Wright inequality in [Rudelson and Vershynin \(2013\)](#), for $\forall a > 0$, there exist constants K_1 and J_1 , such that

$$\mathbb{P}(|\hat{C}_t(i) - C_t(i)| > a) \quad (26)$$

$$= \mathbb{P}(|Y_t^T (U^T A_i U) Y_t - \mathbb{E}[Y_t^T (U^T A_i U) Y_t]| > a \cdot (2m+1-|i_1|)(2m+1-|i_2|)) \quad (27)$$

$$\leq 2 \exp \left(-J_1 \cdot \min \left\{ \frac{a^2 (2m+1-|i_1|)^2 (2m+1-|i_2|)^2}{K_1^4 \|U^T A_i U\|_F^2}, \frac{a (2m+1-|i_1|)(2m+1-|i_2|)}{K_1^2 \|U^T A_i U\|_2} \right\} \right). \quad (28)$$

Next we focus on $\|U^T A_i U\|_F$ and $\|U^T A_i U\|_2$. Since U is an orthogonal matrix,

$$\|U^T A_i U\|_2 = \|A_i\|_2 \leq \|A_i\|_1 = \max_k \sum_{l=1}^{(2m+1)^2} |A_i(k, l)| = 1 \quad (29)$$

and

$$\|U^T A_i U\|_F = \sqrt{\text{Sum of eigenvalues of } (U^T A_i U)^T (U^T A_i U)} \quad (30)$$

$$\leq \sqrt{(2m+1)^2 \cdot \lambda_{\max}((U^T A_i U)^T (U^T A_i U))} \quad (31)$$

$$= \sqrt{(2m+1)^2} \cdot \|U^T A_i U\|_2 \quad (32)$$

$$= 2m+1. \quad (33)$$

Then for $\forall i = (i_1, i_2) \in \mathcal{M}$, there exist constants K_1 , J_1 and J such that

$$\mathbb{P}(|\hat{C}_t(i) - C_t(i)| > a) \quad (34)$$

$$\leq 2 \exp\left(-J_1 \cdot \min\left\{\frac{a^2(2m+1-|i_1|)^2(2m+1-|i_2|)^2}{K_1^4(2m+1)^2}, \frac{a(2m+1-|i_1|)(2m+1-|i_2|)}{K_1^2}\right\}\right) \quad (35)$$

$$\leq 2 \exp(-J \cdot \min\{a^2 m^2, a m^2\}). \quad (36)$$

So when a is small enough, we have

$$\mathbb{P}(|\hat{C}_t(i) - C_t(i)| > a) \leq 2 \exp(-J \cdot a^2 m^2). \quad (37)$$

Next since

$$\|\hat{C}_t - C_t\|_\infty = \max_{i \in \mathcal{M}} |\hat{C}_t(i) - C_t(i)|, \quad (38)$$

by Union bound, for $\forall a > 0$,

$$\mathbb{P}(\|\hat{C}_t - C_t\|_\infty > a) \leq 2(2m+1)^2 \exp(-J \cdot a^2 m^2) \quad (39)$$

$$= 2(2\sqrt{n}+1)^2 \exp(-J \cdot a^2 n). \quad (40)$$

□

Lemma 2.2. *Let $\Delta = \|C^0 - C^1\|_\infty$. Define $\mathcal{A}_k = \{t \in \mathcal{G}_k : \|(\hat{W}\hat{E})_t - C^k\|_\infty \geq \Delta/2\}$, $k = 0, 1$, and $\mathcal{A}' = \mathcal{A}_0 \cup \mathcal{A}_1$, we have $\mathcal{T} \setminus \mathcal{A}' = (\mathcal{G}_0 \setminus \mathcal{A}_0) \cup (\mathcal{G}_1 \setminus \mathcal{A}_1)$. Then all the elements in $\mathcal{T} \setminus \mathcal{A}'$ are clustered correctly.*

Proof. On the one hand, for $\forall t \in \mathcal{G}_0 \setminus \mathcal{A}_0$ and $\forall s \in \mathcal{G}_1 \setminus \mathcal{A}_1$, by contradiction, if $(\hat{W}\hat{E})_t = (\hat{W}\hat{E})_s$,

$$\Delta = \|C^0 - C^1\|_\infty \leq \|C^0 - (\hat{W}\hat{E})_t\|_\infty + \|(\hat{W}\hat{E})_t - (\hat{W}\hat{E})_s\|_\infty + \|(\hat{W}\hat{E})_s - C^1\|_\infty \quad (41)$$

$$< \Delta/2 + 0 + \Delta/2 \quad (42)$$

$$= \Delta, \quad (43)$$

which is conflicted by itself, so $(\hat{W}\hat{E})_t \neq (\hat{W}\hat{E})_s$. On the other hand, suppose $t, s \in \mathcal{G}_0 \setminus \mathcal{A}_0$ or $t, s \in \mathcal{G}_1 \setminus \mathcal{A}_1$, by contradiction, if $(\hat{W}\hat{E})_t \neq (\hat{W}\hat{E})_s$, $\hat{W}\hat{E}$ has at least three distinct rows, however, according to the structure of $\hat{W}\hat{E}$, it has exactly two distinct rows, which is a conflict. So $(\hat{W}\hat{E})_t = (\hat{W}\hat{E})_s$. Thus, all the elements in $\mathcal{T} \setminus \mathcal{A}'$ are clustered correctly. □

Next, we introduce the theory for k-means clustering algorithm.

Theorem 2.3. *Under Assumption 1, 2 and 3, consider k-means clustering in Algorithm 1. For $\forall \beta > 1$, there exists a constant J , as $n \rightarrow \infty$,*

$$\mathbb{P}\left(|\mathcal{R}|/n^2 > \frac{(\log n)^\beta}{\Delta^2 n}\right) \leq 2(2\sqrt{n}+1)^2 n^2 \exp(-J \cdot (\log n)^\beta) \rightarrow 0, \quad (44)$$

where $|\mathcal{R}|/n^2$ is the clustering error rate. Here $\frac{(\log n)^\beta}{\Delta^2 n} \rightarrow 0$ as $n \rightarrow \infty$.

Proof. By Algorithm 1 in Section 2.2, we have

$$\sum_{t \in \mathcal{T}} \|(\hat{W}\hat{E})_t - \hat{C}_t\|_\infty^2 \leq (1 + \epsilon) \cdot \min_{W \in \mathcal{W}_{n,2}, E \in \mathbb{R}_{2 \times (2m+1)^2}} \sum_{t \in \mathcal{T}} \|(WE)_t - \hat{C}_t\|_\infty^2, \quad (45)$$

where $\hat{W} \in \mathcal{W}_{n,2}$, $\hat{E} \in \mathbb{R}_{2 \times (2m+1)^2}$. Without loss of generality, set $\epsilon < 1$, then

$$\sum_{t \in \mathcal{T}} \|(\hat{W}\hat{E})_t - \hat{C}_t\|_\infty^2 \leq (1 + \epsilon) \sum_{t \in \mathcal{T}} \|C_t - \hat{C}_t\|_\infty^2 \quad (46)$$

$$\leq 2 \sum_{t \in \mathcal{T}} \|C_t - \hat{C}_t\|_\infty^2. \quad (47)$$

On the one hand, by Triangle Inequality,

$$\sum_{t \in \mathcal{T}} \|(\hat{W}\hat{E})_t - C_{t0}\|_\infty^2 \leq \sum_{t \in \mathcal{T}} (\|(\hat{W}\hat{E})_t - \hat{C}_t\|_\infty + \|\hat{C}_t - C_t\|_\infty + \|C_t - C_{t0}\|_\infty)^2 \quad (48)$$

$$\leq 3 \sum_{t \in \mathcal{T}} \|(\hat{W}\hat{E})_t - \hat{C}_t\|_\infty^2 + 3 \sum_{t \in \mathcal{T}} \|\hat{C}_t - C_t\|_\infty^2 + 3 \sum_{t \in \mathcal{T}} \|C_t - C_{t0}\|_\infty^2. \quad (49)$$

In addition, by Assumption 3 and (47),

$$\sum_{t \in \mathcal{T}} \|(\hat{W}\hat{E})_t - C_{t0}\|_\infty^2 \leq 6 \sum_{t \in \mathcal{T}} \|C_t - \hat{C}_t\|_\infty^2 + 3 \sum_{t \in \mathcal{T}} \|\hat{C}_t - C_t\|_\infty^2 + 3 \sum_{t \in \mathcal{H}} \|C_t - C_{t0}\|_\infty^2 \quad (50)$$

$$= 9 \sum_{t \in \mathcal{T}} \|\hat{C}_t - C_t\|_\infty^2 + 3 \sum_{t \in \mathcal{H}} \|C_t - C_{t0}\|_\infty^2 \quad (51)$$

$$\leq 9 \sum_{t \in \mathcal{T}} \|\hat{C}_t - C_t\|_\infty^2 + \frac{n(\log n)^\beta}{8}. \quad (52)$$

On the other hand,

$$\sum_{t \in \mathcal{T}} \|(\hat{W}\hat{E})_t - C_{t0}\|_\infty^2 \geq \sum_{t \in \mathcal{A}'} \frac{\Delta^2}{4} = \frac{\Delta^2(|\mathcal{A}_0| + |\mathcal{A}_1|)}{4} = \frac{|\mathcal{A}'|\Delta^2}{4}, \quad (53)$$

then we have

$$|\mathcal{A}'| \leq \frac{36 \sum_{t \in \mathcal{T}} \|\hat{C}_t - C_t\|_\infty^2 + \frac{n(\log n)^\beta}{2}}{\Delta^2}. \quad (54)$$

By Lemma 2.2,

$$\mathbb{P}\left(|\mathcal{R}|/n^2 > \frac{(\log n)^\beta}{\Delta^2 n}\right) = \mathbb{P}\left(|\mathcal{R}| > \frac{n(\log n)^\beta}{\Delta^2}\right) \leq \mathbb{P}\left(|\mathcal{A}'| > \frac{n(\log n)^\beta}{\Delta^2}\right), \quad (55)$$

then by Lemma 2.1 and (54), there exists a constant J ,

$$\mathbb{P}\left(|\mathcal{R}|/n^2 > \frac{(\log n)^\beta}{\Delta^2 n}\right) \quad (56)$$

$$\leq \mathbb{P}\left(\frac{36 \sum_{t \in \mathcal{T}} \|\hat{C}_t - C_t\|_\infty^2 + \frac{n(\log n)^\beta}{2}}{\Delta^2} > \frac{n(\log n)^\beta}{\Delta^2}\right) \quad (57)$$

$$= \mathbb{P}\left(\sum_{t \in \mathcal{T}} \|\hat{C}_t - C_t\|_\infty^2 > \frac{n(\log n)^\beta}{72}\right) \quad (58)$$

$$\leq \sum_{t \in \mathcal{T}} \mathbb{P}\left(\|\hat{C}_t - C_t\|_\infty^2 > \frac{(\log n)^\beta}{72n}\right) \quad (59)$$

$$\leq 2(2\sqrt{n} + 1)^2 n^2 \exp(-J \cdot (\log n)^\beta). \quad (60)$$

So for $\forall \beta > 1$, as $n \rightarrow \infty$,

$$\mathbb{P}\left(|\mathcal{R}|/n^2 > \frac{(\log n)^\beta}{\Delta^2 n}\right) \leq 2(2\sqrt{n} + 1)^2 n^2 \exp(-J \cdot (\log n)^\beta) \rightarrow 0. \quad (61)$$

Thus, for stationary Gaussian random field, we get the error bound of k-means clustering algorithm. \square

3 Non-stationary Textures

In this section we consider textures to be non-stationary. Here both \mathcal{G}_0 and \mathcal{G}_1 are non-stationary Gaussian Markov random fields with mean 0. We add location information into consideration and cluster the n^2 pixels into two groups by single-linkage algorithm. The algorithm is established in Section 3.1. Then we show the consistency of a simple incarnation of the basic approach in Section 3.2.

3.1 Method

Pick up $\lfloor \frac{n}{2m+1} \rfloor \times \lfloor \frac{n}{2m+1} \rfloor$ pixels $\{X_u\}_{u \in \mathcal{U}}$ with equal intervals from $\{X_t\}_{t \in \mathcal{T}}$, where

$$\mathcal{U} = \left\{ u = (u_1, u_2) \mid u_1 = (2m+1) \cdot t_1, \quad u_2 = (2m+1) \cdot t_2, \quad (t_1, t_2) = \left\{ 1, 2, \dots, \left\lfloor \frac{n}{2m+1} \right\rfloor \right\}^2 \right\}. \quad (62)$$

Here \mathcal{U} is a subset of \mathcal{T} . Similar to (2) in Section 2.2, for $\forall u \in \mathcal{U}$, pick up patch S_u as follows

$$S_u = \begin{pmatrix} X_{u+(-m,-m)} & X_{u+(-m,-m+1)} & \cdots & X_{u+(-m,m)} \\ X_{u+(-m+1,-m)} & X_{u+(-m+1,-m+1)} & \cdots & X_{u+(-m+1,m)} \\ \vdots & \vdots & \cdots & \vdots \\ X_{u+(m,-m)} & X_{u+(m,-m+1)} & \cdots & X_{u+(m,m)} \end{pmatrix}. \quad (63)$$

For $\forall u \neq v \in \mathcal{U}$, it is obvious that $|u_1 - v_1| \geq 2m + 1$ or $|u_2 - v_2| \geq 2m + 1$. So there is no overlap between S_u and S_v .

Next for $\forall u \in \mathcal{U}$, add location information into its true feature C_u . Denote C'_u as the new true feature of pixel X_u as follows

$$C'_u = \left(C_u, \frac{u_1}{n}, \frac{u_2}{n} \right), \quad (64)$$

where C'_u is a vector of length $(2m+1)^2 + 2$. Similarly, denote \hat{C}'_u as the new observed feature of pixel X_u as follows

$$\hat{C}'_u = \left(\hat{C}_u, \frac{u_1}{n}, \frac{u_2}{n} \right), \quad (65)$$

where \hat{C}'_u also is a vector of length $(2m+1)^2 + 2$.

Apply single-linkage algorithm in following steps. Firstly among \mathcal{U} , connect all pairs (u, v) with $\|\hat{C}'_u - \hat{C}'_v\|_\infty < \frac{(\log n)^{\beta/2}}{\sqrt{n}}$, where $1 < \beta < 2$. Next for $\forall u \in \mathcal{U}$, assign all the other pixels in S_u into the same cluster as X_u . Then for any pixel X_t which is still not clustered, find the pixel X_u in $\{X_u\}_{u \in \mathcal{U}}$ with the smallest distance to X_t , and assign pixel X_t into the same cluster with X_u . Finally we obtain the clustering result.

As a summary, we provide the procedure of single-linkage algorithm in Algorithm 2.

Algorithm 2 Texture Segmentation with Single-linkage Algorithm

Input: Observations $\{X_t\}_{t \in \mathcal{T}}$.

Output: Single-linkage clustering result.

- 1: For $\forall u = (u_1, u_2) \in \mathcal{U}$, pick up patch S_u .
 - 2: Calculate new observed features $\{\hat{C}'_u\}_{u \in \mathcal{U}}$.
 - 3: Apply single-linkage algorithm based on $\{\hat{C}'_u\}_{u \in \mathcal{U}}$.
 - 4: **return** Single-linkage clustering result.
-

Define the following set

$$\mathcal{V} = \{u \in \mathcal{U} \mid S_u \cap \mathcal{G}_0 = \emptyset \text{ or } S_u \cap \mathcal{G}_1 = \emptyset\} \quad (66)$$

and

$$\mathcal{W} = \{t \in \mathcal{T} \mid X_t \text{ is a pixel in patch } S_u \text{ where } u \in \mathcal{V}\}. \quad (67)$$

In next section, we can show that all the pixels in \mathcal{V} can be clustered correctly with probability going to 1. Thus, all pixels in \mathcal{W} can be clustered correctly with probability going to 1.

3.2 Theory

Firstly we introduce two assumptions on the non-stationary level of the fields.

Assumption 4. For any X_t, X_s in the same sub-region,

$$\|C_t - C_s\|_\infty = O(\sqrt{\log n} \cdot D(s, t)), \quad (68)$$

where $D(s, t)$ is the distance between two pixels X_t and X_s

$$D(s, t) = \sqrt{\left(\frac{s_1 - t_1}{n}\right)^2 + \left(\frac{s_2 - t_2}{n}\right)^2}. \quad (69)$$

Assumption 5. For any X_t, X_s in different sub-regions, if $D(s, t) < \frac{\log n}{\sqrt{n}}$, there exists a constant K such that

$$\|C_t - C_s\|_\infty \geq \frac{K \cdot \log n}{\sqrt{n}}. \quad (70)$$

Next, we show that the single-linkage algorithm in above section is consistent.

Theorem 3.1. *Under Assumption 4 and Assumption 5, by single-linkage clustering in Algorithm 2, set threshold value $b = \frac{(\log n)^{\beta/2}}{\sqrt{n}}$, where $1 < \beta < 2$. Then as $n \rightarrow \infty$,*

$$\mathbb{P}(\text{All pixels in } \mathcal{W} \text{ are clustered correctly}) \geq 1 - n^3 \cdot \exp(-J \cdot (\log n)^\beta) \rightarrow 1. \quad (71)$$

Proof. Set threshold value $b = \frac{(\log n)^{\beta/2}}{\sqrt{n}}$, where $1 < \beta < 2$. For $\forall u \in \mathcal{U}$, denote u_+ as the pixel bordering and above u in \mathcal{U} , and denote u_- as the pixel bordering and below u in \mathcal{U} , then

$$\mathbb{P}(\text{All pixels in } \mathcal{W} \text{ are clustered correctly}) \quad (72)$$

$$\geq 1 - \mathbb{P}\left(\max_{u \in \mathcal{V}} \max_{\substack{v \in \mathcal{V} \\ v, u \text{ in the same sub-region} \\ S_u \text{ borders on } S_v}} \|\hat{C}'_u - \hat{C}'_v\|_\infty > \frac{(\log n)^{\beta/2}}{\sqrt{n}}\right) \quad (73)$$

$$- \mathbb{P}\left(\min_{u \in \mathcal{V}} \min_{\substack{v \in \mathcal{V} \\ v, u \text{ in different sub-regions}}} \|\hat{C}'_u - \hat{C}'_v\|_\infty < \frac{(\log n)^{\beta/2}}{\sqrt{n}}\right) \quad (74)$$

$$- \mathbb{P}\left(\min_{u \in \mathcal{U} \setminus \mathcal{V}} \|\hat{C}'_{u_+} - \hat{C}'_{u_-}\|_\infty < \frac{2(\log n)^{\beta/2}}{\sqrt{n}}\right). \quad (75)$$

By Union bound,

$$\mathbb{P}(\text{All pixels in } \mathcal{W} \text{ are clustered correctly}) \quad (76)$$

$$\geq 1 - \sum_{u \in \mathcal{V}} \sum_{\substack{v \in \mathcal{V} \\ v, u \text{ in the same sub-region} \\ S_u \text{ borders on } S_v}} \mathbb{P}\left(\|\hat{C}'_u - \hat{C}'_v\|_\infty > \frac{(\log n)^{\beta/2}}{\sqrt{n}}\right) \quad (77)$$

$$- \sum_{u \in \mathcal{V}} \sum_{\substack{v \in \mathcal{V} \\ v, u \text{ in different sub-regions}}} \mathbb{P}\left(\|\hat{C}'_u - \hat{C}'_v\|_\infty < \frac{(\log n)^{\beta/2}}{\sqrt{n}}\right) \quad (78)$$

$$- \sum_{u \in \mathcal{U} \setminus \mathcal{V}} \mathbb{P}\left(\|\hat{C}'_{u_+} - \hat{C}'_{u_-}\|_\infty < \frac{2(\log n)^{\beta/2}}{\sqrt{n}}\right). \quad (79)$$

We calculate above probability in three steps. Firstly, under Assumption 4, for $\forall u \in \mathcal{U}$,

$$\max_{\substack{v \in \mathcal{V} \\ v, u \text{ in the same sub-region} \\ S_u \text{ borders on } S_v}} \|C'_u - C'_v\|_\infty = O\left(\sqrt{\frac{\log n}{n}}\right), \quad (80)$$

then by Triangle Inequality,

$$\sum_{u \in \mathcal{V}} \sum_{\substack{v \in \mathcal{V} \\ v, u \text{ in the same sub-region} \\ S_u \text{ borders on } S_v}} \mathbb{P}\left(\|\hat{C}'_u - \hat{C}'_v\|_\infty > \frac{(\log n)^{\beta/2}}{\sqrt{n}}\right) \quad (81)$$

$$\leq \sum_{u \in \mathcal{V}} \sum_{\substack{v \in \mathcal{V} \\ v, u \text{ in the same sub-region} \\ S_u \text{ borders on } S_v}} \left[\mathbb{P}\left(\|\hat{C}'_u - C'_u\|_\infty > \frac{(\log n)^{\beta/2}}{3\sqrt{n}}\right) + \mathbb{P}\left(\|\hat{C}'_v - C'_v\|_\infty > \frac{(\log n)^{\beta/2}}{3\sqrt{n}}\right) \right] \quad (82)$$

$$+ \mathbb{P}\left(\|C'_u - C'_v\|_\infty > \frac{(\log n)^{\beta/2}}{3\sqrt{n}}\right) \quad (83)$$

$$\leq \sum_{u \in \mathcal{V}} \sum_{\substack{v \in \mathcal{V} \\ v, u \text{ in the same sub-region} \\ S_u \text{ borders on } S_v}} \left[\mathbb{P}\left(\|\hat{C}'_u - C'_u\|_\infty > \frac{(\log n)^{\beta/2}}{3\sqrt{n}}\right) + \mathbb{P}\left(\|\hat{C}'_v - C'_v\|_\infty > \frac{(\log n)^{\beta/2}}{3\sqrt{n}}\right) \right]. \quad (84)$$

By Lemma 2.1, for $1 < \beta < 2$, there exists a constant J , as $n \rightarrow \infty$,

$$\sum_{u \in \mathcal{V}} \sum_{\substack{v \in \mathcal{V} \\ v, u \text{ in the same sub-region} \\ S_u \text{ borders on } S_v}} \mathbb{P}\left(\|\hat{C}'_u - \hat{C}'_v\|_\infty > \frac{(\log n)^{\beta/2}}{\sqrt{n}}\right) \quad (85)$$

$$\leq |\mathcal{V}| \cdot 16(2\sqrt{n} + 1)^2 \exp(-J \cdot (\log n)^\beta) \quad (86)$$

$$\leq 16n^2 \exp(-J \cdot (\log n)^\beta) \rightarrow 0. \quad (87)$$

Secondly, for $\forall u, v \in \mathcal{U}$ such that X_u, X_v are in different sub-regions, if $D(u, v) \geq \frac{\log n}{\sqrt{n}}$, then

$$\|C'_u - C'_v\|_\infty \geq \frac{\log n}{2\sqrt{n}}. \quad (88)$$

If $D(u, v) < \frac{\log n}{\sqrt{n}}$, under Assumption 5, there exists a constant K , such that

$$\|C'_u - C'_v\|_\infty \geq \frac{K \cdot \log n}{\sqrt{n}}. \quad (89)$$

So there exists a constant J , as $n \rightarrow \infty$,

$$\sum_{u \in \mathcal{V}} \sum_{\substack{v \in \mathcal{V} \\ v, u \text{ in different sub-regions}}} P\left(\|\hat{C}'_u - \hat{C}'_v\|_\infty < \frac{(\log n)^{\beta/2}}{\sqrt{n}}\right) \quad (90)$$

$$\leq \sum_{u \in \mathcal{V}} \sum_{\substack{v \in \mathcal{V} \\ v, u \text{ in different sub-regions}}} \left[P\left(\|C'_u - C'_v\|_\infty < \frac{3(\log n)^{\beta/2}}{\sqrt{n}}\right) + P\left(\|\hat{C}'_u - C'_u\|_\infty > \frac{(\log n)^{\beta/2}}{\sqrt{n}}\right) \right] \quad (91)$$

$$+ P\left(\|\hat{C}'_v - C'_v\|_\infty > \frac{(\log n)^{\beta/2}}{\sqrt{n}}\right) \quad (92)$$

$$\leq \frac{2n^4}{(2\sqrt{n}+1)^4} \cdot P\left(\|\hat{C}'_u - C'_u\|_\infty > \frac{(\log n)^{\beta/2}}{\sqrt{n}}\right) \quad (93)$$

$$\leq \frac{4n^4}{(2\sqrt{n}+1)^2} \cdot \exp(-J \cdot (\log n)^\beta) \rightarrow 0. \quad (94)$$

Thirdly, for $\forall u \in \mathcal{U} \setminus \mathcal{V}$, X_{u_+} and X_{u_-} are in different sub-regions, so by (88) and (89),

$$\sum_{u \in \mathcal{U} \setminus \mathcal{V}} \mathbb{P}\left(\|\hat{C}'_{u_+} - \hat{C}'_{u_-}\|_\infty < \frac{2(\log n)^{\beta/2}}{\sqrt{n}}\right) = 0. \quad (95)$$

Thus, there exists a constant J , as $n \rightarrow \infty$,

$$P(\text{All pixels in } \mathcal{W} \text{ are clustered correctly}) \quad (96)$$

$$\geq 1 - 16n^2 \exp(-J \cdot (\log n)^\beta) - \frac{4n^4}{(2\sqrt{n}+1)^2} \cdot \exp(-J \cdot (\log n)^\beta) \quad (97)$$

$$\geq 1 - n^3 \cdot \exp(-J \cdot (\log n)^\beta) \rightarrow 1. \quad (98)$$

□

3.3 Example

3.3.1 Model

Follow the ideas in (Higdon et al., 1999), we define non-stationary Gaussian process as follows. For any pixels X_t and X_s , define non-stationary covariance between X_t and X_s to be

$$C(X_t, X_s) = \int_{\mathbb{R}^2} K_t(r) K_s(r) dr, \quad (99)$$

where $K_t(\cdot)$ and $K_s(\cdot)$ are Gaussian kernel functions

$$K_t(r) = \frac{1}{2\pi|\Sigma_t|^{\frac{1}{2}}} \exp\left[-\frac{1}{2}(r-t)^T \Sigma_t^{-1}(r-t)\right] \quad (100)$$

and

$$K_s(r) = \frac{1}{2\pi|\Sigma_s|^{\frac{1}{2}}} \exp\left[-\frac{1}{2}(r-s)^T \Sigma_s^{-1}(r-s)\right]. \quad (101)$$

It is easy to check the covariance is non-negative definite. Then we create the non-stationary process by convoluting the white noise process $\phi(\cdot)$ with kernel function $K_t(\cdot)$,

$$X_t = \int_{\mathbb{R}^2} K_t(r) d\phi(r) \quad \text{for } t \in \mathcal{T}. \quad (102)$$

Next, we simplify the covariance matrix. Suppose $B \sim N(0, \Sigma_t)$ and $D \sim N(s, \Sigma_s)$, where B and D are independent. Let $g_B(\cdot)$, $g_D(\cdot)$ and $g_{D-B}(\cdot)$ denote the density functions of B , D and $D - B$. Similarly, $g_{B,D}(\cdot)$ and $g_{D-B,D}(\cdot)$ are joint density functions. Then

$$C(X_t, X_s) = \int_{\mathbb{R}^2} K_t(r) K_s(r) dr = \int_{\mathbb{R}^2} g_B(r-t) \cdot g_D(r) dr \quad (103)$$

$$= \int_{\mathbb{R}^2} g_{B,D}(r-t, r) dr = \int_{\mathbb{R}^2} g_{D-B,D}(t, r) dr \quad (104)$$

$$= g_{D-B}(t) \cdot \int_{\mathbb{R}^2} g_D(r) dr = g_{D-B}(t). \quad (105)$$

Since $D - B \sim N(s, \Sigma_t + \Sigma_s)$, we have

$$C(X_t, X_s) = g_{D-B}(t) = \frac{1}{2\pi|\Sigma_t + \Sigma_s|^{\frac{1}{2}}} \exp\left[-\frac{1}{2}(t-s)^T(\Sigma_t + \Sigma_s)^{-1}(t-s)\right]. \quad (106)$$

3.3.2 Assumptions and Theory on Example Model

Each pixel X_t has its own kernel function $K_t(\cdot)$, and the non-stationary process is controlled by kernel functions $\{K_t(\cdot)\}_{t \in \mathcal{T}}$. For each pixel X_t , it has Gaussian kernel function

$$K_t(r) = \frac{1}{2\pi|\Sigma_t|^{\frac{1}{2}}} \exp\left[-\frac{1}{2}(r-t)^T \Sigma_t^{-1}(r-t)\right]. \quad (107)$$

The only parameters of the non-stationary process are the covariance matrices $\{\Sigma_t\}_{t \in \mathcal{T}}$ of the kernel functions. Here we call $\{\Sigma_t\}_{t \in \mathcal{T}}$ as the "size" of the kernel functions. If all pixels X_t have the same "size" Σ_t , the field is stationary. For each pixel X_t , $t = (t_1, t_2)$ is a 2-dimension vector, so its "size" Σ_t is a 2×2 matrix. Denote it as

$$\Sigma_t = \begin{pmatrix} a_t & b_t \\ c_t & d_t \end{pmatrix}. \quad (108)$$

For any pixels X_t and X_s , define

$$d(s, t) = \max\{|a_t - a_s|, |b_t - b_s|, |c_t - c_s|, |d_t - d_s|\}. \quad (109)$$

Next, similar to Assumption 4 and Assumption 5, for the example kernel convolution model, we introduce assumptions directly on the "size" of kernel function.

Assumption 6. For $\forall X_t, X_s$ in the same sub-region,

$$d(s, t) = O(\sqrt{\log n} \cdot D(s, t)). \quad (110)$$

Assumption 7. For $\forall X_t, X_s$ in different sub-regions, if $D(s, t) < \frac{\log n}{\sqrt{n}}$, there exists a constant K such that

$$d(s, t) \geq \frac{K \cdot \log n}{\sqrt{n}}. \quad (111)$$

From Lemma A.1, all conditions in Theorem 3.1 are satisfied, so Theorem 3.1 works here. Thus, under Assumption 6 and Assumption 7, single-linkage algorithm is consistent under the example kernel model.

4 Numerical Experiments

In our experiments, for the sake of stability, we use a form of size-constrained k-means (Bradley et al., 2000; Wagstaff et al., 2001), size-constrained single-linkage and size-constrained ward-linkage algorithms.

4.1 Synthetic Stationary Textures

In the section, we create several stationary random field models by moving average on Gaussian noise. Suppose white noise $Z_t \sim N(0, 1)$. We generate four stationary random fields as follows

$$\text{Model 1: } X_t = \sum_{i=-m}^m Z_{t+(i,i)}. \quad (112)$$

$$\text{Model 2: } X_t = \sum_{i=-m}^m Z_{t+(-i,i)}. \quad (113)$$

$$\text{Model 3: } X_t = \sum_{i=-m}^m Z_{t+(0,i)}. \quad (114)$$

$$\text{Model 4: } X_t = \sum_{i=-m}^m Z_{t+(i,0)}. \quad (115)$$

Based on above four models, after standardization and combination, we obtain six 128×128 mosaics, which are showed in Figure 1. Each mosaic contains two different textures, and it is divided by a straight line in the middle.

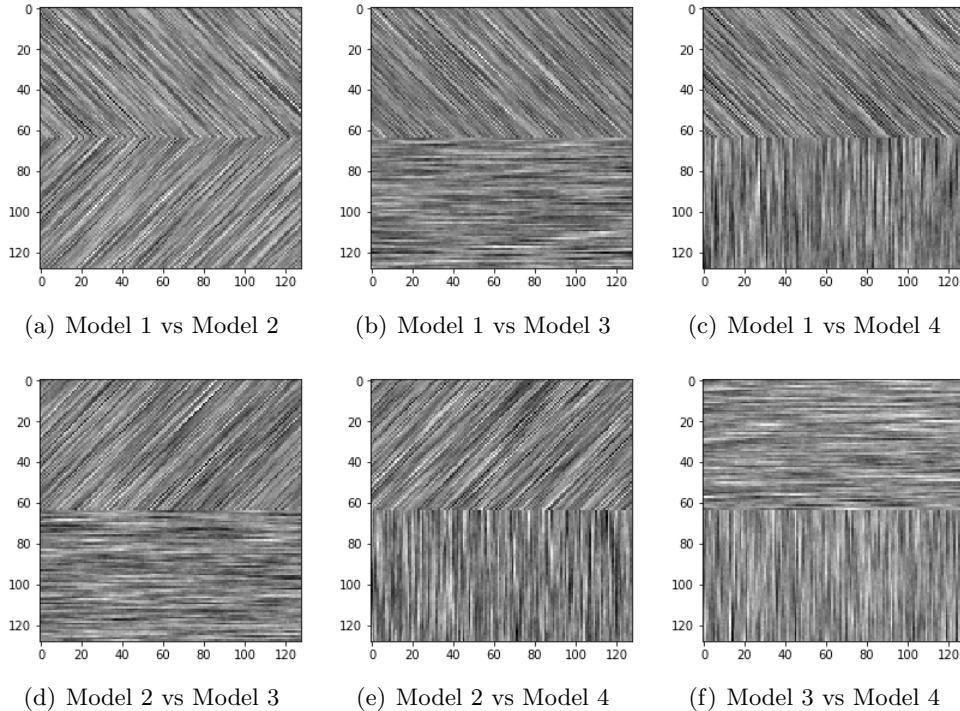


Figure 1: GMRF texture mosaics

We apply $\{\hat{C}'_t\}_{t \in \mathcal{T}}$ as the observed features of pixels $\{X_t\}_{T \in \mathcal{T}}$. Consider three clustering algorithms: size-constrained single-linkage, size-constrained ward-linkage and size-constrained k-means

algorithms. We present segmentation accuracy in Table 1. Single-linkage works but does not perform well, and ward-linkage improves it. K-means algorithm works best and segmentation accuracy is almost 1.

Mosaic	Single-linkage	Ward-linkage	K-means
Model 1 vs Model 2	0.7362	0.9665	0.9868
Model 1 vs Model 3	0.9144	0.9632	0.9820
Model 1 vs Model 4	0.8329	0.9677	0.9867
Model 2 vs Model 3	0.9210	0.9657	0.9822
Model 2 vs Model 4	0.8190	0.9661	0.9868
Model 3 vs Model 4	0.7910	0.9626	0.9816
Mean Value	0.8358	0.9653	0.9844

Table 1: Segmentation accuracy

4.2 Natural Textures

In this section, We pick up textures from Brodatz album (Brodatz, 1966).

4.2.1 Two Regions Divided by a Straight Line

We pick up three textures from Brodatz album (Brodatz, 1966): D_{21} , D_{55} and D_{77} . After standardization and combination, we obtain three 160×160 mosaics, which are showed in Figure 2. Each mosaic contains two different Brodatz textures, and they are divided by a straight line in the middle.

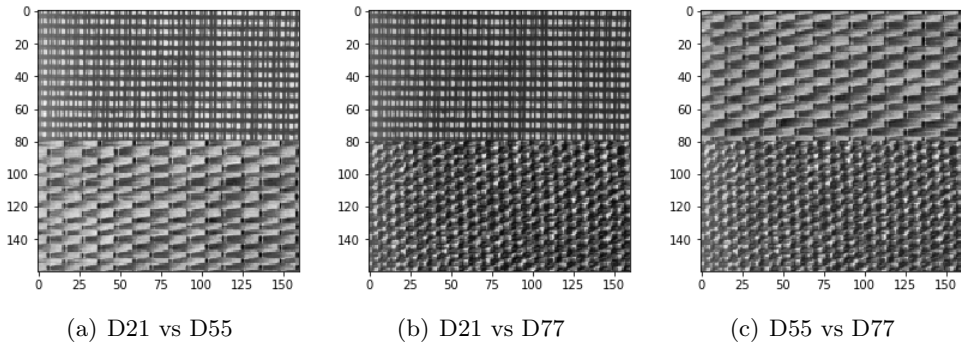
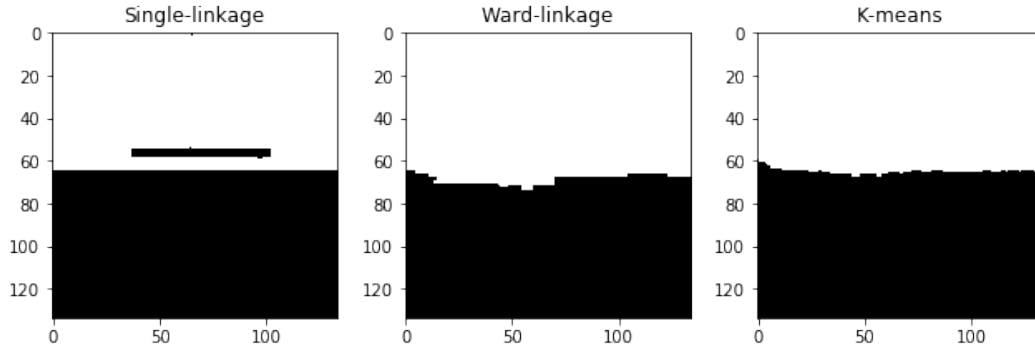
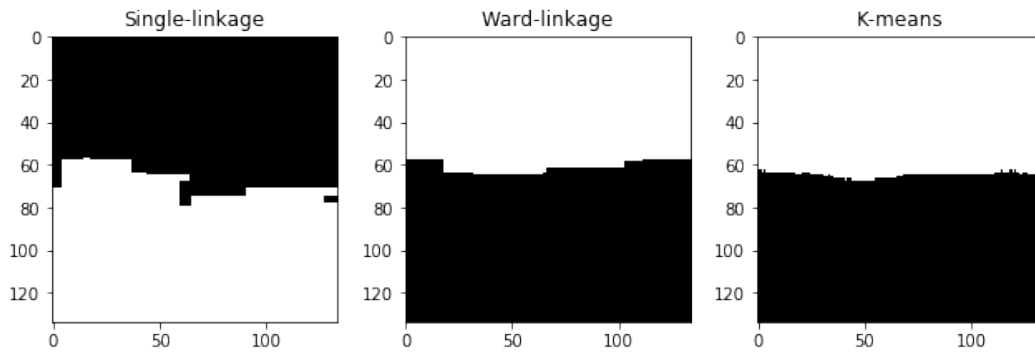


Figure 2: Texture mosaics

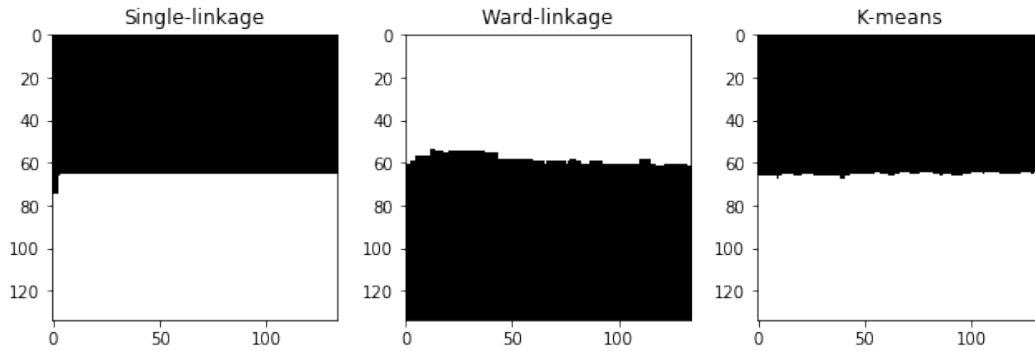
We apply $\{\hat{C}'_t\}_{t \in \mathcal{T}}$ as the observed features of pixels $\{X_t\}_{T \in \mathcal{T}}$. Consider three clustering algorithms: size-constrained single-linkage, size-constrained ward-linkage and size-constrained k-means algorithms. Segmentation results are shown in Figure 3. Also we present segmentation accuracy in Table 2. All three algorithms work perfectly and segmentation accuracy is almost 1.



(a) D21 vs D55



(b) D21 vs D77



(c) D55 vs D77

Figure 3: Segmentation results

Mosaics	Single-linkage	Ward-linkage	K-means
D21 vs D55	0.9703	0.9819	0.9891
D21 vs D77	0.9536	0.9592	0.9858
D55 vs D77	0.9914	0.9396	0.9928
Mean Value	0.9718	0.9602	0.9892

Table 2: Segmentation accuracy

4.2.2 Two Regions Divided by a Curve

Same to Section 4.2.1, we still run simulations on textures $D21$, $D55$ and $D77$. Here in each mosaic, the textures are divided by a circle in the middle, as shown in Figure 4.

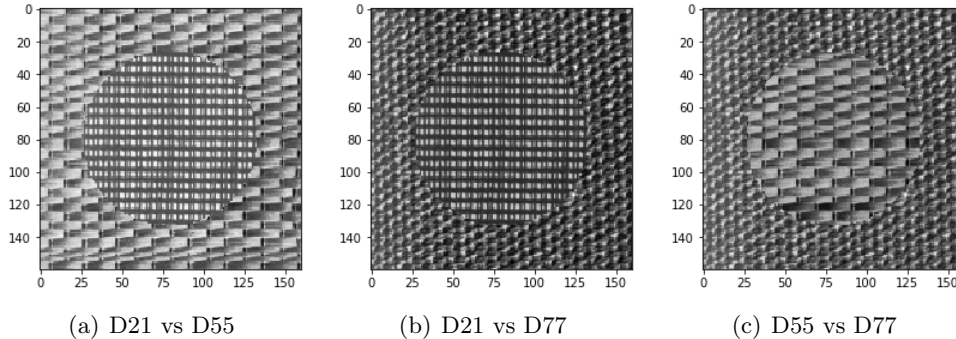


Figure 4: Texture mosaics

We apply $\{\hat{C}'_t\}_{t \in \mathcal{T}}$ as the observed features of pixels $\{X_t\}_{T \in \mathcal{T}}$. Consider three clustering algorithms: size-constrained single-linkage, size-constrained ward-linkage and size-constrained k-means algorithms. Segmentation results are shown in Figure 5. Also we present segmentation accuracy in Table 3. Single-linkage works but does not perform well, and ward-linkage improves it. K-means algorithm works perfectly and segmentation accuracy is almost 1.

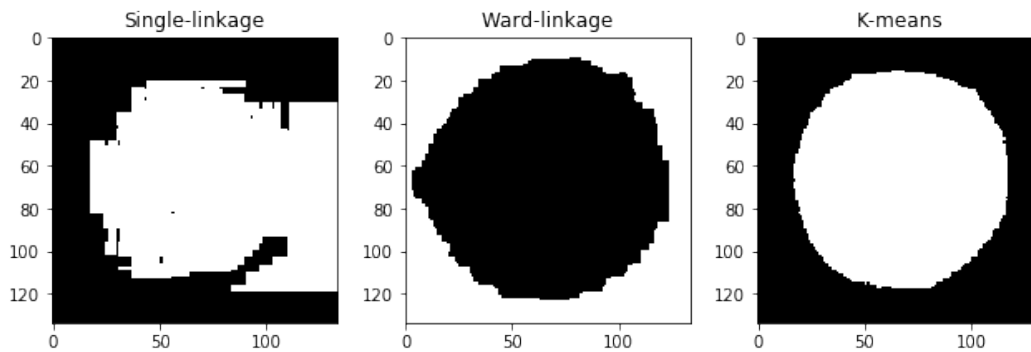
Mosaic	Single-linkage	Ward-linkage	K-means
D21 vs D55	0.8093	0.9332	0.9562
D21 vs D77	0.8903	0.9563	0.9418
D55 vs D77	0.8295	0.8992	0.9739
Mean Value	0.8430	0.9296	0.9573

Table 3: Segmentation accuracy

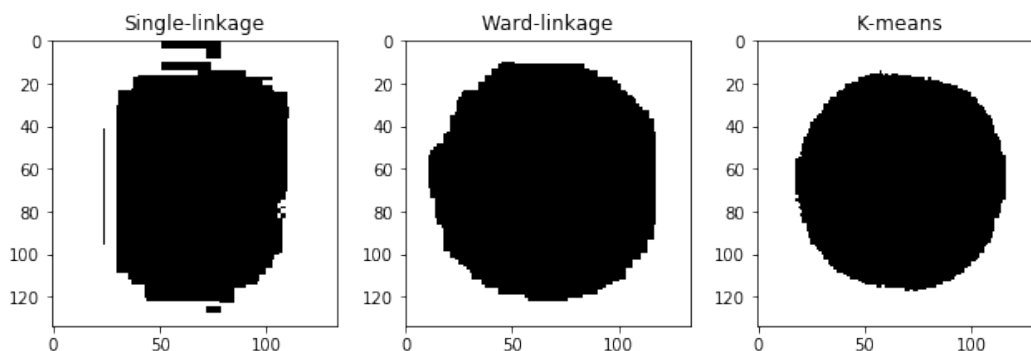
4.2.3 Multiple Regions

Here we construct three mosaics from eight textures in Brodatz album (Brodatz, 1966): $D4$, $D6$, $D20$, $D21$, $D34$, $D52$, $D55$ and $D77$. After standardization and combination, we obtain three 160×160 mosaics, which are showed in Figure 6. Each mosaic contains four different Brodatz textures, and they are divided by horizontal and vertical lines in the middle.

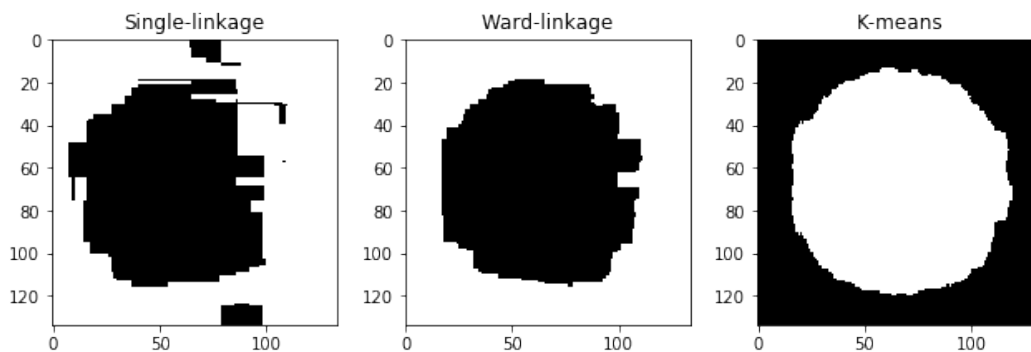
We apply $\{\hat{C}'_t\}_{t \in \mathcal{T}}$ as the observed features of pixels $\{X_t\}_{T \in \mathcal{T}}$. Consider three clustering algorithms: size-constrained single-linkage, size-constrained ward-linkage and size-constrained k-means algorithms. Segmentation results are shown in Figure 7. Also we present segmentation accuracy in Table 4. For multi-cluster mosaics, single-linkage works but does not perform well, and ward-linkage improves it. K-means algorithm works perfectly and segmentation accuracy is almost 1.



(a) D21 vs D55



(b) D21 vs D77



(c) D55 vs D77

Figure 5: Segmentation results

Mosaic	Single-linkage	Ward-linkage	K-means
D04, D06, D20 & D52	0.8478	0.8985	0.9507
D21, D34, D55 & D77	0.7530	0.8969	0.9663
D06, D21, D34 & D77	0.9158	0.8767	0.9465
Mean Value	0.8389	0.8907	0.9545

Table 4: Segmentation accuracy

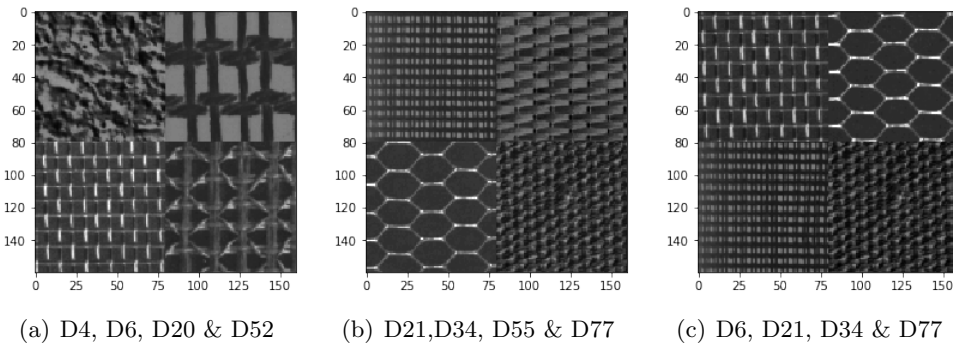


Figure 6: Texture mosaics

5 Discussion

For non-stationary textures, instead of single linkage clustering, we could also use DBSCAN algorithm. When $\text{MinPts} = 2$, DBSCAN is very similar to single-linkage algorithm, but DBSCAN includes a step for removing noisy observations. In this paper, these noisy observations could be the patches that overlap with the edge between the two sub-regions. In practice, in different settings and backgrounds, we can apply different MinPts values in DBSCAN algorithm.

Also in Section 2 and Section 3, we only theoretically show the cases where there are only two sub-regions. Actually when there are more than two regions, the introduced algorithms also work. For example, we indicate the scene with four sub-regions in Section 4.2.3.

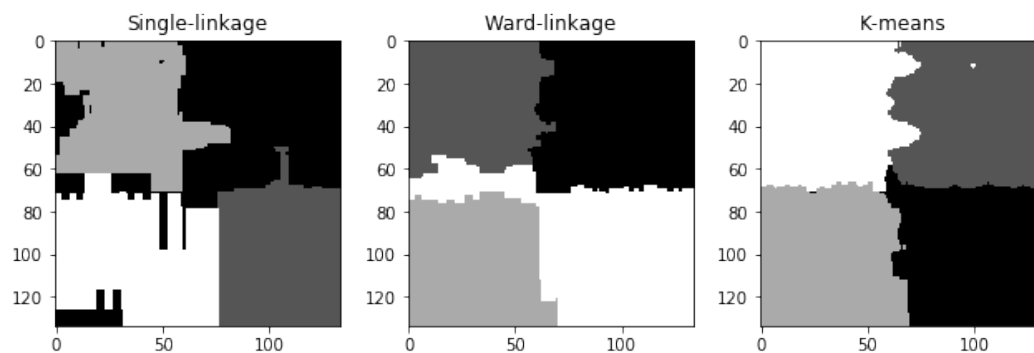
In this paper, we do clustering based on local second moment information on patches. Actually beyond sample autocovariance, we could also use higher-order statistics or other features such as SIFT (Lowe, 1999) for more complex textures that are not necessarily Gaussian, and speculate that similar results could also be obtained in these situations.

Acknowledgments

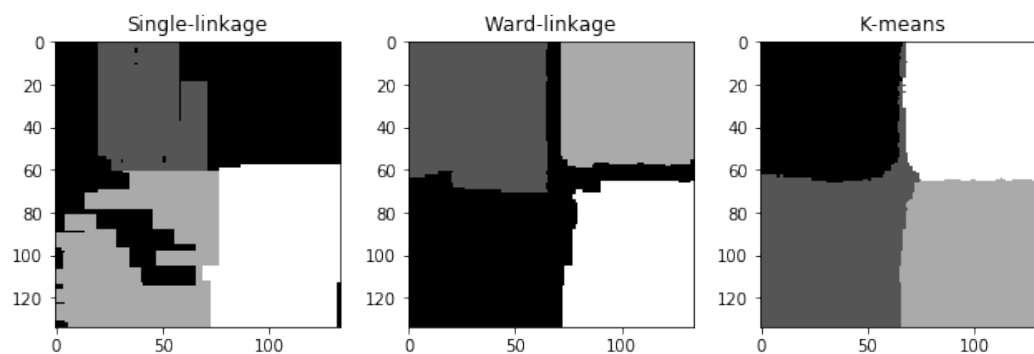
I am grateful to my PhD advisor, Ery Arias-Castro, for suggesting this topic and for his assistance and support throughout this project. I also want to thank Danna Zhang for helpful discussions regarding Gaussian MRFs.

References

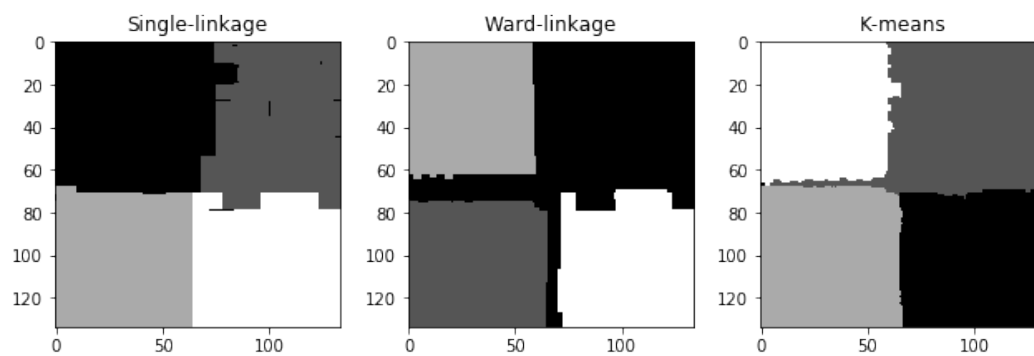
- Arias-Castro, E. (2011). Clustering based on pairwise distances when the data is of mixed dimensions. *IEEE Transactions on Information Theory* 57(3), 1692–1706.
- Arias-Castro, E., S. Bubeck, G. Lugosi, and N. Verzelen (2018). Detecting Markov random fields hidden in white noise. *Bernoulli* 24(4B), 3628–3656.
- Arthur, D. and S. Vassilvitskii (2007). k-means++: The advantages of careful seeding. In *Proceedings of the Eighteenth Annual ACM-SIAM Symposium on Discrete Algorithms. Society for Industrial and Applied Mathematics*, pp. 1027–1035.
- Badrinarayanan, V., A. Kendall, and R. Cipolla (2017). Segnet: A deep convolutional encoder-decoder architecture for image segmentation. *IEEE Transactions on Pattern Analysis and Machine Intelligence* 39(12), 2481–2495.
- Bradley, P. S., K. P. Bennett, and A. Demiriz (2000). Constrained k-means clustering. *Technical Report Microsoft Research, Redmond, WA*.



(a) D04, D06, D20 & D52



(b) D21, D34, D55 & D77



(c) D06, D21, D34 & D77

Figure 7: Segmentation results

- Brodatz, P. (1966). *Textures: A photographic album for artists and designers*. Dover Publications.
- Chellappa, R. and S. Chatterjee (1985). Classification of textures using Gaussian Markov random fields. *IEEE Transactions on Acoustics, Speech, and Signal Processing* 33(4), 959–963.
- Cross, G. R. and A. K. Jain (1983). Markov random field texture models. *IEEE Transactions on Pattern Analysis and Machine Intelligence* 1, 25–39.
- Dasgupta, S. (1999). Learning mixtures of Gaussians. In *40th Annual Symposium on Foundations of Computer Science*, pp. 634–644. IEEE.
- Dasgupta, S. (2010). Hierarchical clustering with performance guarantees. In *Classification as a Tool for Research*, pp. 3–14. Springer.
- Dasgupta, S. and P. M. Long (2005). Performance guarantees for hierarchical clustering. *Journal of Computer and System Sciences* 70(4), 555–569.
- Dunn, D. and W. E. Higgins (1995). Optimal Gabor filters for texture segmentation. *IEEE Transactions on Image Processing* 4(7), 947–964.
- Galun, M., E. Sharon, R. Basri, and A. Brandt (2003). Texture segmentation by multiscale aggregation of filter responses and shape elements. In *Proceedings Ninth IEEE International Conference on Computer Vision*, pp. 716–725. IEEE.
- Geman, S. and C. Graffigne (1986). Markov random field image models and their applications to computer vision. In *Proceedings of the International Congress of Mathematicians*, Volume 1, pp. 1496–1517.
- Grigorescu, S. E., N. Petkov, and P. Kruizinga (2002). Comparison of texture features based on Gabor filters. *IEEE Transactions on Image Processing* 11(10), 1160–1167.
- Higdon, D., J. Swall, and J. Kern (1999). Non-stationary spatial modeling. *Bayesian Statistics* 6(1), 761–768.
- Hofmann, T., J. Puzicha, and J. M. Buhmann (1998). Unsupervised texture segmentation in a deterministic annealing framework. *IEEE Transactions on Pattern Analysis and Machine Intelligence* 20(8), 803–818.
- Hsu, D. and S. M. Kakade (2013). Learning mixtures of spherical Gaussians: moment methods and spectral decompositions. In *Proceedings of the 4th Conference on Innovations in Theoretical Computer Science*, pp. 11–20.
- Humeau-Heurtier, A. (2019). Texture feature extraction methods: A survey. *IEEE Access* 7, 8975–9000.
- Jain, A. K. and F. Farrokhnia (1991). Unsupervised texture segmentation using Gabor filters. *Pattern Recognition* 24(12), 1167–1186.
- Kumar, A., Y. Sabharwal, and S. Sen (2004). A simple linear time $(1 + \epsilon)$ -approximation algorithm for k-means clustering in any dimensions. In *45th Annual IEEE Symposium on Foundations of Computer Science*, pp. 454–462. IEEE.
- Liu, L., J. Chen, P. Fieguth, G. Zhao, R. Chellappa, and M. Pietikäinen (2019). From BoW to CNN: Two decades of texture representation for texture classification. *International Journal of Computer Vision* 127(1), 74–109.
- Long, J., E. Shelhamer, and T. Darrell (2015). Fully convolutional networks for semantic segmentation. In *Proceedings of the IEEE Conference on Computer Vision and Pattern Recognition*, pp. 3431–3440.
- Lowe, D. G. (1999). Object recognition from local scale-invariant features. In *Proceedings of the Seventh IEEE International Conference on Computer Vision*, Volume 2, pp. 1150–1157. IEEE.
- Malik, J., S. Belongie, T. Leung, and J. Shi (2001). Contour and texture analysis for image segmentation. *International Journal of Computer Vision* 43(1), 7–27.
- Manjunath, B. S. and R. Chellappa (1991). Unsupervised texture segmentation using Markov random field models. *IEEE Transactions on Pattern Analysis and Machine Intelligence* 13(5),

- 478–482.
- Mao, J. and A. K. Jain (1992). Texture classification and segmentation using multiresolution simultaneous autoregressive models. *Pattern Recognition* 25(2), 173–188.
- Milletari, F., N. Navab, and S. A. Ahmadi (2016). V-net: Fully convolutional neural networks for volumetric medical image segmentation. In *2016 Fourth International Conference on 3D Vision (3DV)*, pp. 565–571. IEEE.
- Ng, A. Y., M. I. Jordan, and Y. Weiss (2002). On spectral clustering: Analysis and an algorithm. In *Advances in Neural Information Processing Systems*, pp. 849–856.
- Paciorek, C. J. and M. J. Schervish (2006). Spatial modelling using a new class of nonstationary covariance functions. *Environmetrics: The Official Journal of the International Environmetrics Society* 17(5), 483–506.
- Pal, N. R. and S. K. Pal (1993). A review on image segmentation techniques. *Pattern Recognition* 26(9), 1277–1294.
- Randen, T. and J. H. Husoy (1999a). Filtering for texture classification: A comparative study. *IEEE Transactions on Pattern Analysis and Machine Intelligence* 21(4), 291–310.
- Randen, T. and J. H. Husoy (1999b). Texture segmentation using filters with optimized energy separation. *IEEE Transactions on Image Processing* 8(4), 571–582.
- Reed, T. R. and J. H. Dubuf (1993). A review of recent texture segmentation and feature extraction techniques. *CVGIP: Image Understanding* 57(3), 359–372.
- Ronneberger, O., P. Fischer, and T. Brox (2015). U-net: Convolutional networks for biomedical image segmentation. In *International Conference on Medical Image Computing and Computer-Assisted Intervention*, pp. 234–241. Springer.
- Rudelson, M. and R. Vershynin (2013). Hanson-Wright inequality and sub-Gaussian concentration. *Electronic Communications in Probability* 18(82), 1–9.
- Rue, H. and L. Held (2005). *Gaussian Markov random fields: theory and applications*. London: Chapman and Hall–CRC Press.
- Shi, J. and J. Malik (2000). Normalized cuts and image segmentation. *IEEE Transactions on Pattern Analysis and Machine Intelligence* 22(8), 888–905.
- Unser, M. (1995). Texture classification and segmentation using wavelet frames. *IEEE Transactions on Image Processing* 4(11), 1549–1560.
- Varma, M. (2004). *Statistical approaches to texture classification*. Ph. D. thesis, University of Oxford.
- Vempala, S. and G. Wang (2004). A spectral algorithm for learning mixture models. *Journal of Computer and System Sciences* 68(4), 841–860.
- Verzelen, N. (2010a). Adaptive estimation of stationary Gaussian fields. *The Annals of Statistics* 38(3), 1363–1402.
- Verzelen, N. (2010b). High-dimensional Gaussian model selection on a Gaussian design. In *Annales de l’IHP Probabilités et Statistiques*, Volume 46, pp. 480–524.
- Verzelen, N. and F. Villers (2009). Tests for Gaussian graphical models. *Computational Statistics & Data Analysis* 53(5), 1894–1905.
- Wagstaff, K., C. Cardie, S. Rogers, and S. Schrödl (2001). Constrained k-means clustering with background knowledge. In *Proceedings of the Eighteenth International Conference on Machine Learning*, Volume 1, pp. 577–584.
- Weldon, T. P. and W. E. Higgins (1996). Design of multiple Gabor filters for texture segmentation. In *1996 IEEE International Conference on Acoustics, Speech, and Signal Processing Conference Proceedings*, Volume 4, pp. 2243–2246. IEEE.
- Zhang, Y. J. (2006). *Advances in image and video segmentation*. IRM Press.
- Zhu, S. C., Y. Wu, and D. Mumford (1998). Filters, random fields and maximum entropy (FRAME):

A Miscellanea

A.1 Auxiliary results

Lemma A.1. For any pixels X_t, X_s in the image,

$$\|C_t - C_s\|_\infty = O(d(s, t)). \quad (116)$$

Proof. For any pixel X_t and $\forall i = (i_1, i_2) \in \mathcal{M}$,

$$C_t(i) = \text{Mean value of } \{C(X_t, X_{t+i}) \mid \text{both } X_t \text{ and } X_{t+i} \text{ are in } S_t\}. \quad (117)$$

Also we have

$$C(X_t, X_{t+i}) \quad (118)$$

$$= \frac{1}{(2\pi)^2 |\Sigma_t + \Sigma_{t+i}|^{\frac{1}{2}}} \cdot \exp\left(-\frac{1}{2} \left(\frac{i}{n}\right) (\Sigma_t + \Sigma_{t+i})^{-1} \left(\frac{i}{n}\right)^T\right) \quad (119)$$

$$= \frac{1}{(2\pi)^2 \left| \begin{pmatrix} a_t + a_{t+i} & b_t + b_{t+i} \\ c_t + c_{t+i} & d_t + d_{t+i} \end{pmatrix} \right|^{\frac{1}{2}}} \cdot \exp\left(-\frac{1}{2} \left(\frac{i}{n}\right) \begin{pmatrix} a_t + a_{t+i} & b_t + b_{t+i} \\ c_t + c_{t+i} & d_t + d_{t+i} \end{pmatrix}^{-1} \left(\frac{i}{n}\right)^T\right) \quad (120)$$

$$= \frac{1}{(2\pi)^2 \sqrt{(a_t + a_{t+i})(d_t + d_{t+i}) - (b_t + b_{t+i})(c_t + c_{t+i})}}. \quad (121)$$

$$\exp\left(-\frac{1}{2(a_t + a_{t+i})(d_t + d_{t+i}) - (b_t + b_{t+i})(c_t + c_{t+i})} \left(\frac{i}{n}\right) \begin{pmatrix} d_t + d_{t+i} & -b_t - b_{t+i} \\ -c_t - c_{t+i} & a_t + a_{t+i} \end{pmatrix} \left(\frac{i}{n}\right)^T\right). \quad (122)$$

$$(123)$$

For $\forall t \in \mathcal{T}$ and $i \in \mathcal{M}$, let

$$I_{t,i} = (a_t + a_{t+i})(d_t + d_{t+i}) - (b_t + b_{t+i})(c_t + c_{t+i}), \quad (124)$$

then

$$C(X_t, X_{t+i}) \quad (125)$$

$$= \frac{1}{(2\pi)^2 \sqrt{I_{t,i}}} \cdot \exp\left(-\frac{1}{2I_{t,i}} \left(\frac{i}{n}\right) \begin{pmatrix} d_t + d_{t+i} & -b_t - b_{t+i} \\ -c_t - c_{t+i} & a_t + a_{t+i} \end{pmatrix} \left(\frac{i}{n}\right)^T\right). \quad (126)$$

Also for $\forall t \in \mathcal{T}$ and $i \in \mathcal{M}$, let

$$R_{t,i} = \frac{1}{(2\pi)^2 \sqrt{I_{t,i}}} \quad (127)$$

and

$$Q_{t,i} = \exp\left(-\frac{1}{2I_{t,i}} \left(\frac{i}{n}\right) \begin{pmatrix} d_t + d_{t+i} & -b_t - b_{t+i} \\ -c_t - c_{t+i} & a_t + a_{t+i} \end{pmatrix} \left(\frac{i}{n}\right)^T\right), \quad (128)$$

then

$$C(X_t, X_{t+i}) = R_{t,i} \cdot Q_{t,i}. \quad (129)$$

Similarly, for any pixel $X_s \neq X_t$,

$$C(X_s, X_{s+i}) = R_{s,i} \cdot Q_{s,i}. \quad (130)$$

Next, we work on the bound of $|C(X_t, X_{t+i}) - C(X_s, X_{s+i})|$. Since

$$|R_{t,i} - R_{s,i}| = \left| \frac{1}{(2\pi)^2 \sqrt{I_{t,i}}} - \frac{1}{(2\pi)^2 \sqrt{I_{s,i}}} \right| = O(d(s, t)) \quad (131)$$

and

$$|Q_{t,i} - Q_{s,i}| = Q_{t,i} \cdot O\left(\frac{d(s, t)}{n}\right) = O\left(\frac{d(s, t)}{n}\right), \quad (132)$$

we have

$$|C(X_t, X_{t+i}) - C(X_s, X_{s+i})| = |R_{t,i} \cdot Q_{t,i} - R_{s,i} \cdot Q_{s,i}| \quad (133)$$

$$\leq R_{t,i} \cdot |Q_{t,i} - Q_{s,i}| + Q_{s,i} \cdot |R_{t,i} - R_{s,i}| \quad (134)$$

$$\leq O\left(\frac{d(s, t)}{n}\right) + O(d(s, t)) \quad (135)$$

$$= O(d(s, t)). \quad (136)$$

Then for any pixels X_t, X_s in the image, for $\forall i \in \mathcal{M}$,

$$|C_t(i) - C_s(i)| = O(d(s, t)). \quad (137)$$

Thus,

$$\|C_t - C_s\|_\infty = O(d(s, t)). \quad (138)$$

□